Available online at www.sciencedirect.com
SCIENCE DIRECT®
Composites: Part A 36 (2005) 1094–1101
composites
Part A: applied science and manufacturing
www.elsevier.com/locate/compositesa

Polypropylene/talc/SEBS (SEBS-*g*-MA) composites. Part 1. Structure

Matjaž Denac[a,*], Ivan Šmit[b], Vojko Musil[a]

[a]*University of Maribor, Faculty of Economics and Business, Institute of Technology, Razlagova 14, 2000, Maribor Slovenia*
[b]*Ruđer Bošković Institute, 10000 Zagreb, Croatia*

Received 8 December 2004; accepted 10 January 2005

Abstract

Isotactic polypropylene/styrenic rubber block copolymer blends (iPP/SRBC) as well as the iPP/talc/SRBC composites with 12 vol% of aminosilane surface treated talc were studied by optical and scanning electron microscopy, and by wide angle X-ray diffraction. Structure of polypropylene blends and composites was investigated as a function of poly(styrene-*b*-ethylene-*co*-butylene-*b*-styrene) triblock copolymer (SEBS) and the SEBS grafted with maleic anhydride (SEBS-*g*-MA) content in the range from 0 to 20 vol% as elastomeric components. Both copolymers (SEBS and SEBS-*g*-MA) affected the iPP spherulite size in blends by nucleation and solidification effects during crystallization. Talc crystals, homogeneously incorporated in the iPP matrix, accommodated mostly plane-parallel to the surface of the samples and strongly affected crystallization process of the iPP matrix disturbing well-developed spherulitic morphology of polypropylene. Both, SEBS and SEBS-*g*-MA block copolymers, encapsulated talc crystals, thus forming core–shell morphology in significantly higher extent than the poly(styrene-*b*-butadiene-*b*-styrene) triblock (SBS) and the poly(styrene-*b*-ethylene-*co*-propylene) diblock copolymer (SEP) in iPP/talc composites, studied previously. SEBS-*g*-MA encapsulated and disorientated plane-parallel talc crystals more significantly than the SEBS block copolymer.

Keywords: A. Polymer-matrix composites (PMCs); A. Particle-reinforcement; B. Microstructure; Isotactic polypropylene

1. Introduction

Polypropylene (PP) is quite an outstanding polymeric material with respect to its performance, in particular its wide property spectrum, easy processability, versatility of applications and attractive combination of favourable economics. However, its application as an engineering thermoplastic is somewhat limited because of its relatively poor impact resistance, especially at low temperatures. To improve impact toughness of the PP, it is common practice to incorporate elastomers, but its stiffness and strength are thus simultaneously reduced. On the other hand, rigid inorganic particles, i.e. fillers, mostly improve the stiffness, strength, hardness, and abrasion resistance of the PP, but they usually reduce its impact strength [1,2].

Commonly used iPP/talc composites have been widely researched polypropylene composites [3–10]. However, the iPP/talc composites, modified by styrenic rubber block copolymers (SRBC) have been rarely investigated [11–14].

To improve the profile of the mechanical properties of the iPP/talc composites, we examined these composites as modified with certain types of SRBC. In previous paper [15], we compared the structure–property relationships of the iPP/talc composites, modified with poly(styrene-*b*-ethylene-*co*-propylene) diblock copolymer (SEP) and poly(styrene-*b*-butadiene-*b*-styrene) triblock copolymer (SBS), with the ones of the corresponding iPP/SRBC blends. In present research, we compared the efficiency of non-functionalized poly(styrene-*b*-ethylene-*co*-buthylene-*b*-styrene) (SEBS) and SEBS functionalized with maleic anhydride (SEBS-*g*-MA) (thermoplastic elastomers) as impact modifiers and coupling agents (encapsulation efficiency) for the iPP/aminosilanized talc composites. By comparing the influential effects of two block copolymers on the same constitutional basis on the structure and mechanical properties of the blends and composites, the information about blending and encapsulation efficiency of these copolymers could be obtained. Because several authors reported [16–19] that SEBS strongly effects

* Corresponding author. Tel.: +386 2 2290 234; fax: +386 2 2527 056.
E-mail address: matjaz.denac@uni-mb.si (M. Denac).

1359-835X/$ - see front matter © 2005 Elsevier Ltd. All rights reserved.
doi:10.1016/j.compositesa.2005.01.022

the nucleation, crystallization rate, orientation and spherulite growth of the matrix iPP phase, it is very interesting to examine how functionalised SEBS-*g*-MA copolymer affects the crystallization process in the iPP matrix. According to these aims, the effects of the SEBS and SEBS-*g*-MA content upon the structure of the iPP/talc/SRBC composites and the corresponding iPP/SRBC blends are presented and discussed in this paper.

2. Experimental

2.1. Materials

An isotactic PP (BASF), an aminosilane surface treated lamellar talc (Luzenac) and a poly(styrene-*b*-ethylene-*co*-butylene-*b*-styrene) block copolymer (SEBS) as well as a SEBS grafted with maleic anhydride (SEBS-*g*-MA) as polymer matrix and modifiers were used in this study, respectively. The characteristics of the iPP and modifiers are listed in Table 1 as received, while the molecular weights were additionally determined by size-exclusion chromatography.

2.2. Sample preparation

Binary iPP/SEBS and iPP/SEBS-*g*-MA blends with volume content ratios 97.5/2.5, 95/5, 90/10 and 80/20 vol%, as well as ternary iPP/talc/SEBS and iPP/talc/SEBS-*g*-MA composites with the same SRBC volume fractions (content in vol%) and with 12 vol% of added talc were prepared in a Brabender kneading chamber. The components with certain prescription were kneaded for 6 min in a chamber, preheated to 200 °C, with a rotor speed 50 min^{-1}. The melt was transferred to a laboratory press and compression molded into 1- and 4-mm plates. The pressing temperature was 220 °C, pressure 100 bar, pressing time 14 min for 1-mm and 9.5 min for 4-mm thick plates. Afterwards, the plates were cooled to ambient temperature.

2.3. Optical microscopy

To establish polarizing micrographs, a Leica light microscope with a digital camera was used for observation of thin cross-microtomed sections of 1-mm thick plates. Because of the arising polygonal spherulite forms, the maximal anisotropic diameter of the spherulites (d_{max}) was measured on several polarization micrographs of each sample and was quantified as a number average of a spherulite diameter (d_{sph}) of each sample by Eq. (1)

$$d_{sph} = \frac{\sum N_i d_{i,max}}{\sum N_i} \quad (1)$$

where N_i is the number of the measured spherulites with the maximal diameter $d_{i,max}$.

2.4. Scanning electron microscopy (SEM)

A scanning electron microscope (SEM) Jeol JSM 840-A was used to study the morphology.

Samples were cooled in liquid nitrogen and fractured after that. The SEM micrographs were taken from the fractured surfaces of the samples, as well as from the fractured surfaces of the samples, etched with xylene, at the room temperature. Micrographs were taken at the acceleration voltage of 10 kV and magnifications of 2000 and 9000-times.

2.5. Wide-angle X-ray diffraction (WAXD)

The wide-angle X-ray diffractograms of the 1-mm thick plates were taken by a Philips diffractometer PW1710, with monochromatized Cu K_α radiation in the diffraction range $2\theta = 5–40°$. An orientation parameter C, used as a measure for orientation of the corresponding (040) α-iPP planes, was calculated by Eq. (2) proposed by Zipper et al. [20]

$$C = \frac{I_{040}}{I_{110} + I_{040} + I_{130}} \quad (2)$$

where I represents the intensities of the corresponding reflections.

3. Results and discussion

3.1. Polarization microscopy

Micrographs of the pure iPP, blends and composites are shown in Fig. 1. Polarizing micrograph of the pure

Table 1
Properties of materials used

Material	Mark	Trade name (source)	Properties
Isotactic polypropylene	iPP	Novolen 1100 L (BASF)	MFI = 6 g/10 min, $\rho = 0.908$ g/cm^3, $M_n = 47{,}000$, $M_w/M_n = 9.3$
Talc with aminosilane surface treated (2%)	T-V592	Talk Naintsch A-20 V592 (Luzenac)	Particle size (top cut) = 20 μm, $\rho = 2.8$ g/cm^3, specific surface = 6.5 m^2/g
Block copolymer poly(styrene-*b*-ethylene-*co*-butylene-*b*-styrene)	SEBS	Kraton G-1651 (Shell)	$M_n = 162{,}300$, $M_w/M_n = 1.20$ w(PS) = 33%
Block copolymer poly(styrene-*b*-ethylene-*co*-butylene-*b*-styrene) grafted with maleic anhydride	SEBS-*g*-MA	Kraton KG-1901 (Shell)	$M_n = 47{,}300$, $M_w/M_n = 1.55$, w(PS) = 29%, w(MA) = 2%

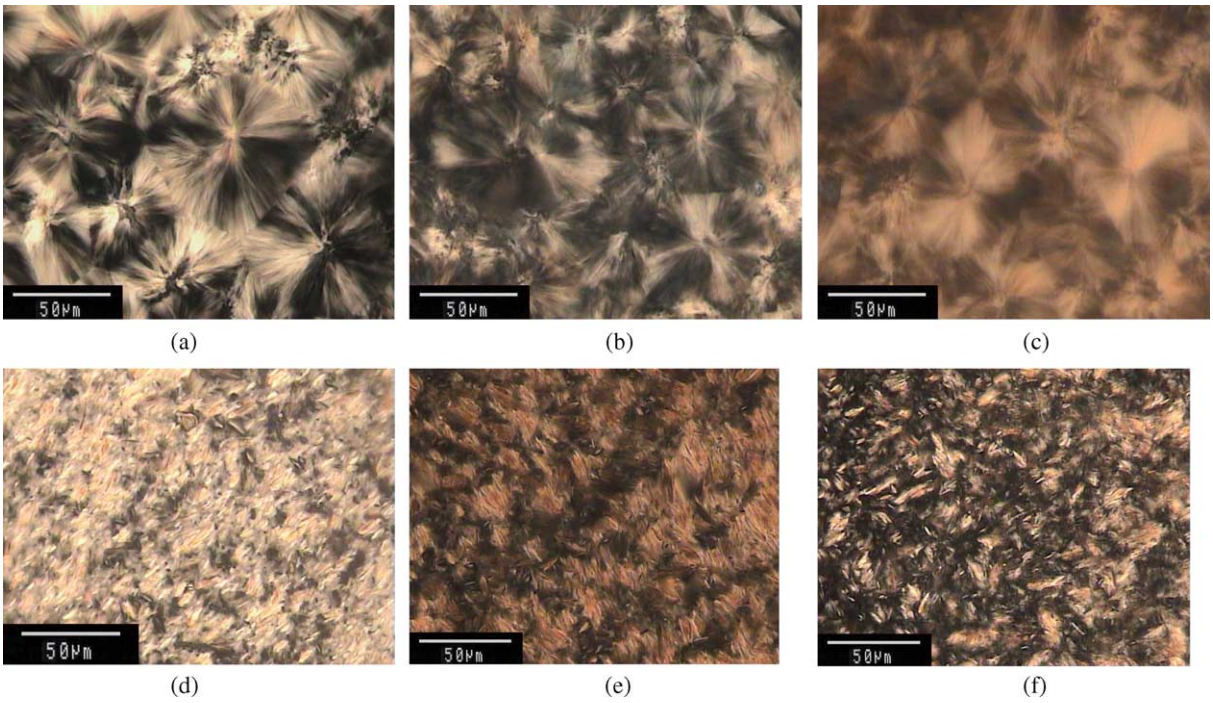

Fig. 1. Polarizing micrographs of pure iPP, iPP blends, iPP/talc composites and ternary composites with SEBS and SEBS-*g*-MA; iPP (a); iPP/SEBS (90/10) (b); iPP/SEBS-*g*-MA (90/10) (c); iPP/talc (88/12) (d); iPP/talc/SEBS (78/12/10) (e); iPP/talc/SEBS-*g*-MA (78/12/10) (f). (For interpretation of the reference to color in this legend, the reader is referred to the web version of this article.)

iPP reveals uniform, well-developed spherulitic morphology with radial, mostly polygonal, α-spherulites and without transcrystal layers (Fig. 1a). Such uniform morphology is usual for compression-molded iPP, as opposite to distinctive skin-core layers in injection-molded iPP, firstly proved by Kantz [21]. The addition of SEBS and SEBS-*g*-MA to the iPP causes a rather complex morphology consisting of radial spherulites within the sample, and transcrystal layers at the surfaces (Fig. 1b and c). Transcrystalline layers (α-cylindritic) in the present compression molded iPP/SEBS and iPP/SEBS-*g*-MA blends may be a consequence of an increased extent of under-cooling ($\Delta T_c = T_m - T_c$) and an increased density extent of the nuclei [16–18,22,23]. Gupta and Purwar [16] have shown that small amounts of the SEBS elastomer caused the under-cooling effect in the iPP matrix, by decreasing of onset and peak of crystallization exotherm. Such rapid cylindric crystallization proceeding on row nuclei, which were formed during solidification, could form a transcrystalline layer even in compression-molded iPP [24,25]. Although the nucleation in the iPP is most effective at the iPP–SEBS interface [17], the SEBS copolymer could also act as heterogeneous nuclei, because it exists in the form of micelles (or micellar clusters) in the iPP/SEBS blends with up to 10 wt% of SEBS [18,19]. Setz et al. [19] have explained the appearance of transcrystal layers in compression-molded iPP/SEBS blends by high nucleation ability of SEBS at the interface with the iPP phase.

Fig. 2 presents an average spherulite diameter (d_{sph}) in iPP and blends, in dependence on styrene-rubber block-copolymer (SRBC) content. Lower amounts of SEBS and SEBS-*g*-MA, nucleate crystallization of iPP by decreasing

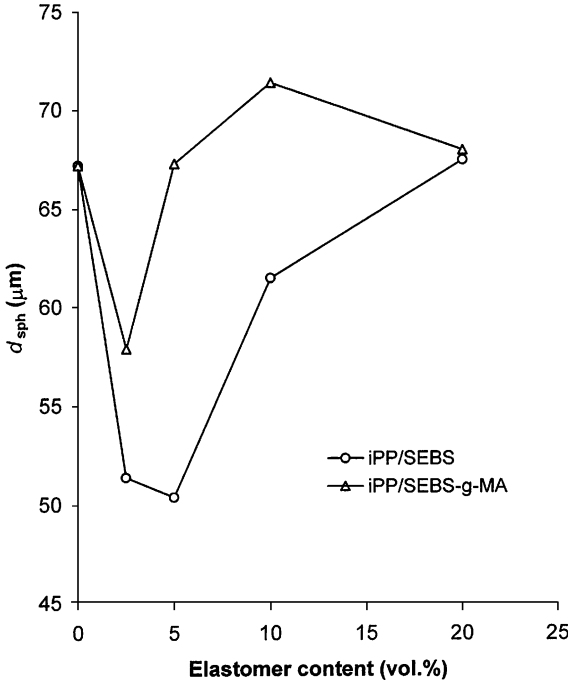

Fig. 2. Average diameter of spherulites for iPP/SEBS and iPP/SEBS-*g*-MA blends.

the spherulite size. Long et al. have proven nucleation ability of SEBS in the iPP/SEBS blends in a quantitative way [17]. Minimal spherulite diameters at 5 vol% of added copolymers (Fig. 2) are in good agreement with maximal extent of under-cooling at about 5 wt% of SEBS observed by Gupta and Purwar [16]. Further addition of SEBS and SEBS-*g*-MA causes the increase of spherulite diameters (Fig. 2).

Such enlarging of the spherulite size (at higher SEBS and SEBS-*g*-MA amounts) seems to be caused by different factors in solidification process that prevail nucleation ability of SEBS and SEBS-*g*-MA. The most effective ones seem to be the interactions at the iPP–SEBS and iPP–SEBS-*g*-MA interfaces (because of good compatibility between the iPP chains and E/B blocks), which may affect lamellar growth [19].

This factor, more effective in the iPP/SEBS-*g*-MA than in iPP/SEBS blends, causes greater spherulites in the iPP/SEBS-*g*-MA blends, because of the fact that SEBS-*g*-MA has lower molecular weight (consequently lower viscosity) than SEBS, and because of stronger interactions in iPP–SEBS-*g*-MA than in iPP–SEBS. Similar enlarging of spherulites by adding the SBS and SEP block copolymers to iPP was observed in previous studies [15,24,25].

The incorporation of talc into pure iPP and into iPP/SEBS and iPP/SEBS-*g*-MA blends disturbs well-developed spherulites (Fig. 1d–f). Polarization micrographs of composites exhibit thin, dark branched iPP grains (nodules), without the Maltese cross. Obviously, talc affects nucleation of the α-iPP phase and hinders well-developed spherulitization in the iPP matrix. It is very interesting that the talc crystals mostly do not shine at any position of the polars, i.e. they are not brilliant neither under polarization nor visible light (Fig. 1e and f). Talc crystals, overlapped with brown colored elastomer mass, seem to be encapsulated by the SEBS and SEBS-*g*-MA elastomers. It seems that the encapsulation in the iPP/talc/SEBS-*g*-MA composites is present in greater extent; talc particles are covered with thin elastomer layers and become disoriented with the addition of the SEBS-*g*-MA. In the composites with SEBS, only bigger talc particles are partially or completely encapsulated with thick elastomer interlayers, but significant disorientation of encapsulated particles is not observed. Both, the iPP/talc/SEBS and iPP/talc/SEBS-*g*-MA composites exhibit more expressive core–shell effect in comparison with the iPP/talc/SBS and iPP/talc/SEP composites. In the latter, micrographs mainly reveal the brilliancy of talc crystals [15]. Polarizing micrographs of all composites reveal homogenous distribution of separated talc crystals without agglomeration. Talc crystals in the iPP/talc/SEBS composites orientate preferentially plane-parallel to the compression-molded surface, whereas they exhibit some degree of disorientation in the iPP/talc/SEBS-*g*-MA composites (Fig. 1f). Stronger disorientation of talc crystals in the iPP/talc/SEBS-*g*-MA composites may be caused by lower molecular weight of the SEBS-*g*-MA in comparison with SEBS (considerably lower melt viscosity), and/or by stronger talc–SEBS-*g*-MA (or iPP–SEBS-*g*-MA) than talc–SEBS (or iPP–SEBS) interactions.

3.2. Scanning electron microscopy

Scanning electron micrographs of fractured samples are presented on Figs. 3–5. SEM micrographs on Fig. 3 confirm homogeneous distribution of the SRBC and talc particles in the iPP matrix phase. Dispersed SEBS particles in iPP have spherical form with an average diameter up to 2 μm. SEBS-*g*-MA forms finer dispersion (particles up to 1 μm) as a result of lower molecular weight (Table 1) and consequently, of higher melt flow index (MFI) in comparison to SEBS (Fig. 3a and b). Coalescence occurs with the increase of SRBC content, therefore dispersed SRBC particles become more irregular in shape. Dispersed SRBC particles still exist on the broken surface of unetched samples, or they are torn out of the matrix without a marked deformation, thus indicating a weak adhesion between the SRBC and iPP matrix (Fig. 4).

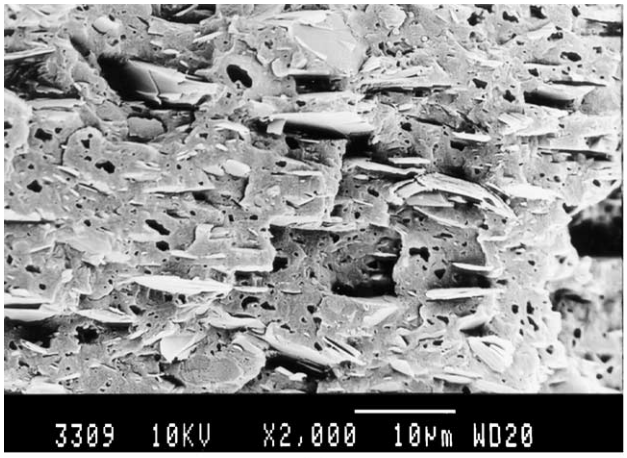

(a)

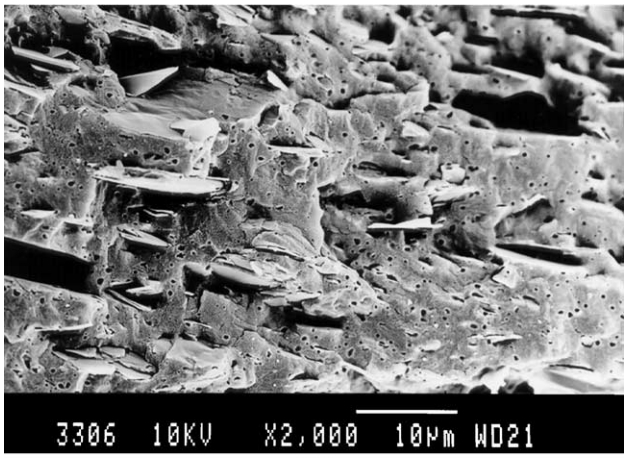

(b)

Fig. 3. SEM micrographs of xylene etched iPP composites; iPP/talc/SEBS (78/12/10) (a); iPP/talc/SEBS-*g*-MA (78/12/10) (b).

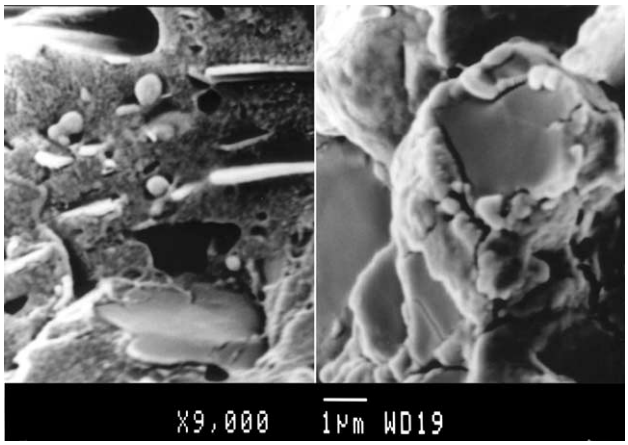

Fig. 4. SEM micrographs of unetched iPP composites; iPP/talc/SEBS (78/12/10) (left); iPP/talc/SEBS-*g*-MA (78/12/10) (right).

Plate-like talc crystals are mostly accommodated plane-parallel to the sample surface. During the compression molding of the sample into a plate, they orientated in the melt flow direction. SEM micrographs also reveal a homogeneous particle distribution of both incorporated components without noticeable agglomeration. The break of the samples surface is gradual and brittle, because the talc particles are mostly pulled out of the iPP matrix at break (Figs. 3–5).

Dispersed SEBS particles are randomly distributed in relation to talc in ternary iPP/talc/SEBS composites, whereas dispersed SEBS-*g*-MA particles are more often located on the talc surface in the iPP/talc/SEBS-*g*-MA composites (Figs. 4 and 5). Talc crystals are partially or completely encapsulated by SEBS-*g*-MA, forming the so called core–shell morphology. A very illustrative example of core–shell morphology of the unetched and etched sample surface of the iPP/talc/SEBS-*g*-MA composites with talc crystals encapsulated by white, more diffused SEBS-*g*-MA layer, is presented in Fig. 4. Micrographs of etched iPP/talc/SEBS-*g*-MA sample confirmed additionally the presence of core–shell morphology (Fig. 5). Only few

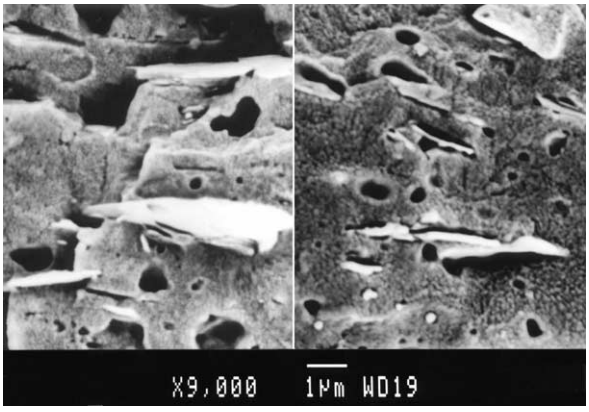

Fig. 5. SEM micrographs of xylene etched iPP composites; iPP/talc/SEBS (78/12/10) (left); iPP/talc/SEBS-*g*-MA (78/12/10) (right).

authors have reported about core–shell morphology in ternary composites [26–28]. They found that core–shell morphology is influenced by several parameters:

- by changing the processing conditions during the preparation of the composites [26];
- unsaturated (SBS, SIS) elastomers are able to form core–shell morphology differently from the saturated (EPDM, EPR, SEBS) [27]. Stricker et al. [28] confirmed presumption of Stamhuis et al. by finding that only unsaturated SEBS-*g*-MA formed core–shell morphology in the study of ternary iPP/talc/SEBS and iPP/talc/SEBS-*g*-MA composites.

In the present work, core–shell morphology in the iPP/talc/SEBS-*g*-MA composites is confirmed by SEM as well as by optical microscopy. Optical micrographs of the iPP/talc/SEBS composites also reveal the covering of talc crystals by SEBS elastomer, implying the encapsulation of talc by SEBS, but in lower extent (Fig. 6). Although saturated SEBS elastomer should not be able to form core–shell morphology according to Stamhuis rule, SEBS somewhat encapsulates talc crystals probably because of its high molecular weight (higher than for polypropylene). As was revealed by optical microscopy, talc crystals are covered with thin SEBS-*g*-MA layers in the iPP/talc/SEBS-*g*-MA composites, whereas in the iPP/talc/SEBS composites only bigger talc particles are partially or completely encapsulated with thick SEBS interlayer. Thicker SEBS than SEBS-*g*-MA interphase layer is conceivable because of lower interactivity and three-times higher molecular weight (related with melt flow index) of the SEBS than SEBS-*g*-MA elastomer.

3.3. WAXD

In diffractograms of the iPP/SEBS and iPP/SEBS-*g*-MA blends (Fig. 7), as well as in diffractograms of binary and ternary composites (Fig. 8), mainly a stable monoclinic α-phase iPP appears. The absence of β-phase (absence of 300 β reflection) in binary and ternary iPP composites is expected, because talc has a strong α-nucleating effect [29]. The addition of SEBS or SEBS-*g*-MA to iPP does not noticeably affect β-nucleation in comparison to SEP diblock copolymer as a strong β nucleator [25]. The incorporation of SRBC, and especially talc filler, into the iPP matrix changes the reflection intensity of the α-phase of iPP, i.e. the ingredients affect the orientation of α-form crystallites. The incorporation of talc into the iPP/SRBC blends gradually depresses the 110 reflection and intensifies the 040 reflection of α-iPP, whereas the addition of SEBS-*g*-MA exhibits a contrary effect (Fig. 8).

Talc filler and elastomers exhibit opposite influence on the orientation parameter *C* (defined by Eq. (2)) (Fig. 9). The addition of SEBS and SEBS-*g*-MA to iPP somewhat decreases *C* values (somewhat expressive for SEBS-*g*-MA)

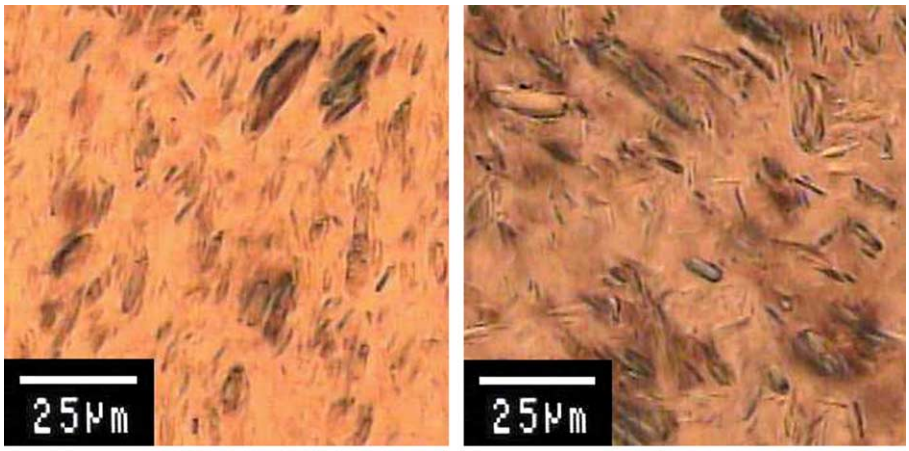

Fig. 6. Polarizing micrograph details of encapsulation for ternary iPP composites; iPP/talc/SEBS (68/12/20) (a); iPP/talc/SEBS-*g*-MA (68/12/20) (b).

thus increasing, according to Zipper et al. [20], *c*-axis orientation. The incorporation of talc into the iPP matrix gradually increases *C* values up to 0.92. According to Zipper et al., $C=1$ corresponds to pure *a**-axis orientation [20], and high $C=0.92$ value indicates a rise of high *a**-axis-orientation by introducing talc. Lovinger revealed that *a**-axis is the axial direction of lamellar growth and a preferred radial growth of spherulites [30]. Moreover, Fujiyama et al. [31] showed that *a**-axis-oriented lamellae are parallel to the sample surface. Obviously, plane-parallel accommodated talc crystals affect the growth of plane-parallel *a**-axis orientation of the α-iPP lamellae. The addition of SEBS block copolymer to the iPP/talc composites affects *C* values negligibly, i.e. the iPP/talc/SEBS composites still exhibit high plane-parallel *a**-axis orientation of the α-iPP lamellae. It corresponds well with mostly plane-parallel oriented talc crystals in micrographs of the iPP/talc/SEBS composites. The addition of the SEBS-*g*-MA to composites intensifies the 110 reflection and depresses 040 α-iPP reflection (Fig. 8) and therefore decreases *C* index significantly (Fig. 9). SEBS-*g*-MA suppresses *a**-axis orientation, thus balancing bimodal *c*- and *a**-axis orientation. Obviously, some extent of disoriented talc crystals in polarization micrographs of

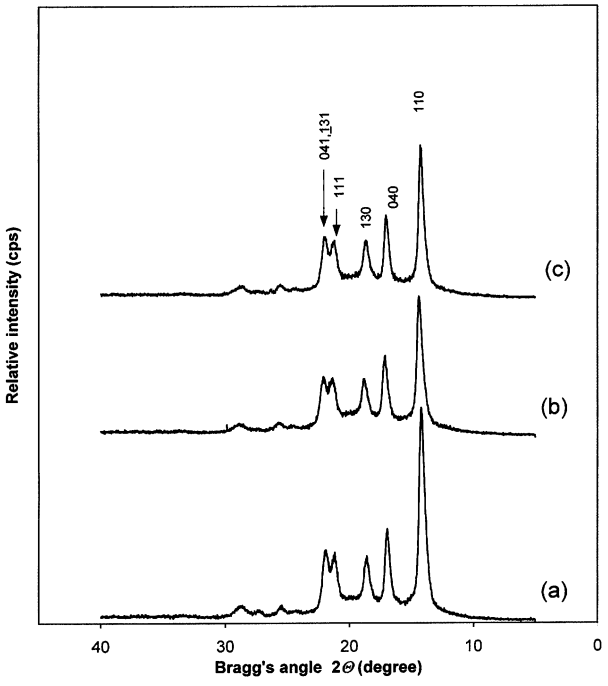

Fig. 7. WAXD diffractograms of selected samples of iPP and iPP blends; iPP (a); iPP/SEBS (90/10) (b); iPP/SEBS-*g*-MA (90/10) (c).

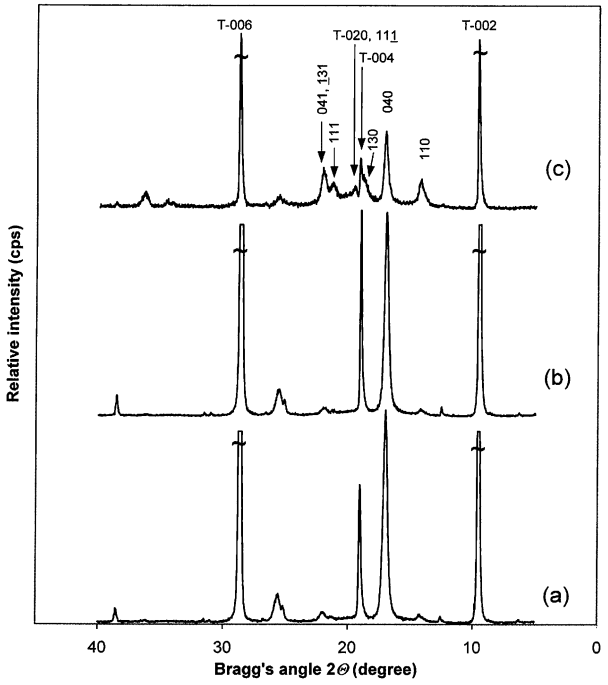

Fig. 8. WAXD diffractograms of selected samples of binary and ternary iPP composites; iPP/talc (88/12) (a); iPP/talc/SEBS (78/12/10) (b); iPP/talc/SEBS-*g*-MA (78/12/10) (c).

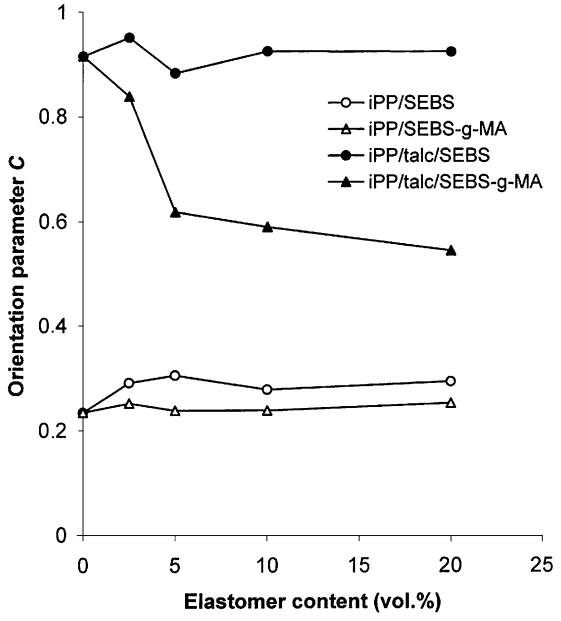

Fig. 9. Dependence of orientation *C* parameter of iPP blends and composites on elastomer content.

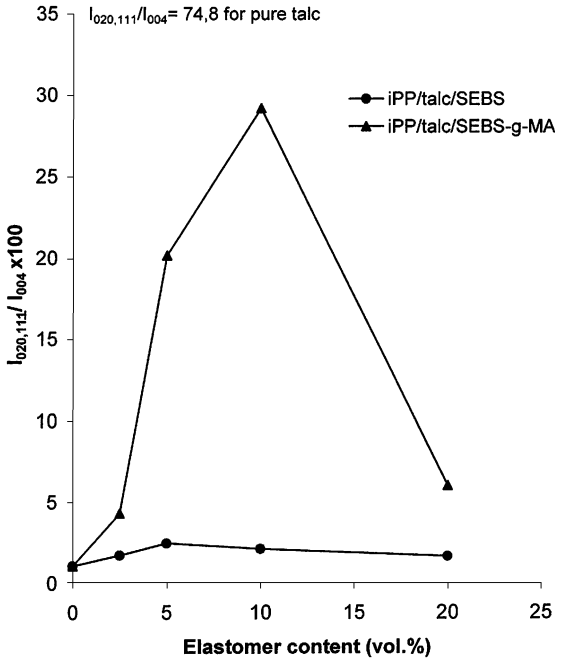

Fig. 10. Dependence of intensity ratio $I_{020,11\underline{1}}/I_{004}$ of corrresponding talc reflections on elastomer content.

the iPP/talc/SEBS-*g*-MA composites (see Fig. 1f) causes some degree of disorientation of the α-iPP lamellae.

The intensity of talc reflections in diffractograms also changes by introducing of talc into pure iPP or by introducing SEBS and SEBS-*g*-MA into iPP/talc, thus implying reorientation of talc crystals in the iPP matrix. In comparison to the pure talc, the intensities of talc reflections in the iPP/talc composite change significantly. *00l* reflections remain strong, whereas the intensity of some *hkl* reflections, like 020, 11$\underline{1}$ peak, decreases. Talc V-592 crystals have monoclinic symmetry with the *C*2/*c* space group (Card No. 3-0881) [32]. Taking into account the intensity of reflections, a diffractogram of applied talc is closer to the Card No. 13-558 [33] and 29-1493 [34]. Card No. 13-558 [33] is applied for indexing of talc reflections in Fig. 8.

Fig. 10 shows very low ratio intensity of two neighboring reflections $I_{020,11\underline{1}}/I_{004}$ after introducing talc into pure iPP, thus confirming strong plane-parallel orientation of talc in the iPP plate. The addition of SEBS does not change this intensity relationship, whereas the addition of SEBS-*g*-MA increases the $I_{020,11\underline{1}}/I_{004}$ value significantly (especially at 10 vol% of SEBS-*g*-MA). The increase of the $I_{020,11\underline{1}}/I_{004}$ intensity relationship is in good accordance with previous results (polarization micrographs and *C* index) and confirms strong influence of SEBS-*g*-MA on the reorientation of plane-parallel talc crystals in the iPP matrix. Because of higher activity and lower molecular weight of SEBS-*g*-MA than SEBS elastomer, SEBS-*g*-MA causes stronger randomizing effect on talc filler.

4. Conclusions

Binary iPP/SEBS and iPP/SEBS-*g*-MA blends exhibited complex morphology consisting of radial spherulites within the sample and transcrystalline layers at the surfaces. Both copolymers affected spherulite size in the iPP matrix by nucleation and solidification during the crystallization of polypropylene blends. While SEBS copolymer affected nucleation in the iPP matrix more strongly, decreasing the spherulite size, SEBS-*g*-MA affected solidification process more significantly, increasing the spherulite size. The incorporation of talc into pure iPP and iPP blends disturbed well-developed spherulitic morphology. Homogeneously incorporated talc crystals accommodated mostly plane-parallel in the iPP matrix, thus affecting the crystallization of polypropylene composites and the orientation of α-iPP lamellae. Polarization and SEM micrographs revealed that both, SEBS and SEBS-*g*-MA block copolymers, encapsulated talc crystals, thus forming core–shell morphology. SEBS-*g*-MA elastomer encapsulated and disoriented plane-parallel talc crystals more expressively than the SEBS block copolymer. In the iPP/talc/SEBS composites, only bigger talc crystals were partially or completely encapsulated with thicker SEBS interlayers. Both, the iPP/talc/SEBS and iPP/talc/SEBS-*g*-MA composites, exhibited expressive core–shell effect in comparison with the iPP/talc/SBS and iPP/talc/SEP composites studied previously. Core–shell effect (encapsulation extent of talc crystals) in the iPP/talc/SRBC composites seemed to decrease in the SEBS-*g*-MA > SEBS > SBS > SEP row, affected by different factors. Among them, the interactivity of elastomer with

filler (stronger at activated and unsaturated elastomer macromolecules) and molecular weight (influencing melt flow index and interlayer thickness) seemed to be most influencing in the studied iPP/talc/SRBC composites.

Acknowledgements

The authors are grateful to the Ministry of Education, Science and Sport of the Republic of Slovenia and to the Ministry of Science and Technology of the Republic Croatia for the financial support.

References

[1] Stricker F, Friedrich C, Mülhaupt R. Influence of morphology on rheological and mechanical properties of SEBS-toughened, glass-bead-filled isotactic polypropene. J Appl Polym Sci 1998;69: 2499–506.
[2] Denac M, Musil V. The influence of thermoplastic elastomers on morphological and mechanical properties of PP/talc composites. Acta Chim Sloven 1999;49:55–67.
[3] Martinatti F, Ricco T. High-rate fracture toughness of polypropylene-based, hybrid, particulate composites. J Mater Sci 1994;29:442–8.
[4] Taranco J, Martinez JMG, Laguna O, Collar EP. Polypropylene/talc composites: interfacial modifications by surface treatments on the solid particles. J Polym Eng 1994;13(4):287–304.
[5] Švehlova V, Polouček E. Mechanical properties of talc-filled polypropylene. Influence of filler content, filler particle size and quality of dispersion. Angew Makromol Chem 1994;214:91–9.
[6] Pukanszky B, Maurer FHJ. Composition dependence of the fracture toughness of heterogeneus polymer systems. Polymer 1995;36(8): 1617–25.
[7] Velasco JI, De Saja JA, Martinez AB. Crystallization behavior of PP filled with surface-modified talc. J Appl Polym Sci 1996;61:125–32.
[8] Hohenberger W. Neueste Trends bei Füllstoffen. Kunststoffe 1997;87: 1106–12.
[9] Wypych G. Handbook of fillers. 2nd ed. Toronto: ChemTec Publishing; 1999. p. 395–460.
[10] Naiki M, Fukui Y, Matsumura T, Nomura T, Matsuda M. Effect of talc on the crystallization of isotactic polypropylene. J Appl Polym Sci 2001;79:1693–703.
[11] Stamhuis JE. Mechanical properties and morphology of polypropylene composites III. Short glass fiber reinforced elastomer modified polypropylene. Polym Compos 1988;9(4):280–4.
[12] Stricker F, Mülhaupt R. Compatibilized polypropylene hybrid composites: influence of elastomeric interlayers on mechanical properties and nucleation behavior. High Perform Polym 1996;8: 97–108.
[13] Long Y, Shanks RA. PP/elastomer/filler hybrids. II. Morphologies and fracture. J Appl Polym Sci 1996;62:639–46.
[14] Stricker F, Maier RD, Mülhaupt R. The influence of metallocene based LLDPE on PP compounds in the presence of SEBS and talcum. Angew Makromol Chem 1998;256:95–9.
[15] Denac M, Musil V, Šmit I. Structure and mechanical properties of talc-filled blends of polypropylene and styrenic block copolymers. J Polym Sci Polym Phys 2004;4:1255–64.
[16] Gupta AK, Purwar SN. Crystallization of PP in PP/SEBS blends and its correlation with tensile properties. J Appl Polym Sci 1984;29: 1595–609.
[17] Long Y, Shanks RA, Stachursky ZH. Kinetics of polymer crystallization. Prog Polym Sci 1995;20:651–701.
[18] Plawky U, Wenig W. Structure and crystallization behaviour of polyolefin blends. Macromol Symp 1996;102:183–90.
[19] Setz S, Stricker F, Kessler J, Duschek T, Mülhaupt R. Morphology and mechanical properties of isotactic or syndiotactic polypropylene with SEBS block copolymers. J Appl Polym Sci 1996;59:1117–28.
[20] Zipper P, Janosi A, Wrentschur E, Knabl C, Abuja PM. Ortsaufgelöste Röntgenbeugung an Kunsstoff-Formteilen II. Darstellung von Formteilquerschnitten durch Weitwinkelmessungen mittels eines ortsemplindlichen Detektors. Österr Kunststoff-Zeitschrift 1993;24:162–5.
[21] Kantz MR, Newman Jr HD, Stigale FH. The skin-core morphology and structure property relationships in injection-molded polypropylene. J Appl Polym Sci 1972;16:1249–60.
[22] Greco R, Coppola F. Influence of crystallization conditions on the mechanical properties of isotactic polypropylene. Plast Rubber Process Appl 1986;6:35–41.
[23] Varga J. Supermolecular structure of isotactic polypropylene. J Mater Sci 1992;27:2557–79.
[24] Šmit I, Radonjič G. Effects of SBS on phase morphology of iPP/aPS blends. Polym Eng Sci 2000;40:2144–60.
[25] Radonjič G, Šmit I. Phase morphology and mechanical properties of iPP/SEP blends. J Polym Sci Polym Phys 2001;39:566–80.
[26] Ou YC, Guo TT, Fang XP, Yu ZZ. Toughening and reinforcing polypropylene with core–shell structured fillers. J Appl Polym Sci 1999;74:2397–403.
[27] Stamhuis JE. Mechanical properties and morphology of polypropylene composites. Talc-filled, elastomer-modified polypropylene. Polym Compos 1984;5:202–7.
[28] Stricker F, Mülhaupt R. Compatibilized polypropylene hybrid composites: influence of elastomeric interlayers on mechanical properties and nucleation behaviour. High Perform Polym 1996;8: 97–108.
[29] Varga J, Schulek Toth F, Mudra I. Blends of the β-modification of polypropylene. Macromol Symp 1994;78:229–41.
[30] Lovinger AJ. Microstructure and unit-cell orientation in α-polypropylene. J Polym Sci Polym Phys Ed 1983;21:97–110.
[31] Fujiyama M, Wakino T, Kawasaki Y. Structure of skin layer in injection-molded polypropylene. J Appl Polym Sci 1988;35:29–49.
[32] Powder Diffraction File, ICDD, JCPDS, Swarthmore, Pa. (Card No. 3-0881).
[33] Powder Diffraction File, ICDD, JCPDS, Swarthmore, Pa. (Card No. 13-558).
[34] Powder Diffraction File, ICDD, JCPDS, Swarthmore, Pa. (Card No. 29-1493).